



# Marine alga “*Bifurcaria bifurcata*”: biosorption of Reactive Blue 19 and methylene blue from aqueous solutions

Said Bouzikri<sup>1</sup> · Nadia Ouasfi<sup>1</sup> · Naoual Benzidia<sup>1</sup> · Anas Salhi<sup>1</sup> · Salem Bakkas<sup>1</sup> · Layachi Khamliche<sup>1</sup>

Received: 22 November 2019 / Accepted: 23 January 2020 / Published online: 6 February 2020  
© Springer-Verlag GmbH Germany, part of Springer Nature 2020

## Abstract

In this study, we have investigated the removal efficiency of two organic pollutants: methylene blue (MB) and Reactive Blue 19 (RB19) dyes by using a brown marine alga abundantly available on the Moroccan coastlines called *Bifurcaria bifurcata* (Bif-Bcata). During the experiments that were conducted in batch mode, we have studied the effect of some parameters such as pH, Bif-Bcata mass, contact time, and initial dye concentration in order to optimize the most suitable biosorption conditions. The biosorption tests on Bif-Bcata showed that the equilibrium is reached after 15 min for both dyes MB and RB19. The optimal pH values are 5.6 and 1.0 for MB and RB19, respectively. Kinetic studies revealed that the biosorption of both dyes follows the pseudo-second-order model. The biosorption isotherms demonstrated that the Langmuir model is the most appropriate to describe the biosorption equilibrium for both dyes MB and RB19 with maximum biosorption capacities reaching 2744.5 mg/g for MB and 88.7 mg/g for RB19. According to these results, it is clear that Bif-Bcata can be considered a promising biomaterial to be used as an effective biosorbent for the elimination of cationic and anionic dyes from textile effluents.

**Keywords** Biosorption · Alga · *Bifurcaria bifurcata* · Methylene blue · Reactive Blue 19

## Introduction

The development of various anthropogenic activities, industrialization and excessive urbanization, and environmental pollution by various effluents has become a major ecological problem (Ait Ahsaine et al. 2018). Water, considered the most important natural resource in the world, is increasingly threatened by the pollution because of organic and inorganic toxic substances that are released directly into the aquatic environment: oceans and rivers (Zbair et al. 2018d, 2019a). Synthetic dyes are organic compounds used extensively in textile, leather, paper, food, pigments, plastics, and cosmetic industries to color the produced matter (Lakshmipathy and Sarada 2016). In fact, the different dyes released into aquatic environments are qualified either as direct toxic or protoxic substances that can lead to other dangerous derivatives after their

metabolization. As a result, they are at the origin of several pathologies such as skin allergy and irritation and can even be carcinogenic (DeVito 1993; Ganesh et al. 1994; Ben Mansour et al. 2007, 2009). For that, it is necessary to implement the appropriate techniques for treating these pollutants. Several methods were used for this purpose. Due to the low biodegradability of dyes, biological treatment processes are not very efficient for their decolorization; hence, they are generally treated by physicochemical techniques (Mafra et al. 2013) such as adsorption on activated carbon, ultrafiltration, electro-dialysis, advanced oxidation processes, and reverse osmosis (Ait Ahsaine et al. 2016; Zbair et al. 2018c; Haffad et al. 2019; Anfar et al. 2019). Unfortunately, the last ones are less adaptable and more expensive, which has encouraged researchers to find out other alternative techniques. In fact, biosorption is considered a “cost-effective technique” for the treatment of colored water (Lakshmipathy and Sarada 2016; Tran and Chao 2018). Many biosorbent materials have been used to remove dyestuffs, including watermelon rind (*Citrullus lanatus*) (Lakshmipathy and Sarada 2016), fly ash and bottom ash (Aarfane et al. 2014a), orange peel (Lazim et al. 2015), spent tea leaves (Lazim et al. 2015), Moroccan date pits (Badri et al. 2018), and brown seaweed (*Sargassum muticum*) (El Atouani et al. 2019).

Responsible editor: Tito Roberto Cadaval Jr

✉ Layachi Khamliche  
Khamliche@yahoo.fr

<sup>1</sup> Chemistry Department, Faculty of Science, Laboratory of Organic Chemistry, Bioorganic and Environment, University Chouaib Doukkali, El Jadida, Morocco

In the objective of natural resources valorization (Benzidia et al. 2015, 2017; Ouasfi et al. 2019a, 2019b), for the removal the cationic and anionic organic pollutants, we have proposed to study the biosorption capability of textile dyes by using algal biomass as a biosorbent which is of great interest, due to its efficiency, abundance, and affordable cost. We, therefore, selected the brown alga *Bifurcaria bifurcata* (Bif-Bcata), a widely available biomaterial on Moroccan coasts, to study the biosorption ability of two dyes: methylene blue (MB) and Reactive Blue 19 (RB19) which are cationic and anionic dyes, respectively.

During this study, we have determined the optimal conditions for the biosorption of MB and RB19 onto Bif-Bcata by studying the influence of the following parameters: pH, Bif-Bcata mass, contact time, initial dye concentration. The kinetic study and the modeling of biosorption isotherms were also examined using appropriate models.

## Materials and methods

### Adsorbate molecules

Methylene blue is a cationic dye belonging to the thiazine group, whereas Reactive Blue 19 is an anionic dye being part of the anthraquinone family. Their main characteristics are given in Table 1. The stock solution of methylene blue and Reactive Blue 19 was prepared by dissolving a mass of 1 g in 1 L of distilled water. Then, a series of dilutions are made in order to obtain appropriate concentrations.

### Preparation of the biosorbent material

The *Bifurcaria bifurcata* (Bif-Bcata) alga was collected from the Sidi Bouzid site in El Jadida city during the low tide period. Once arrived at the laboratory, it was washed with water, dried in a ventilated place and then in the oven at 60 °C for 24 h, and crushed and sieved to obtain a size of 0.5 mm. Figure 1 shows the raw material obtained.

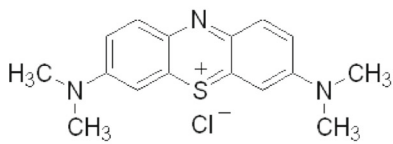
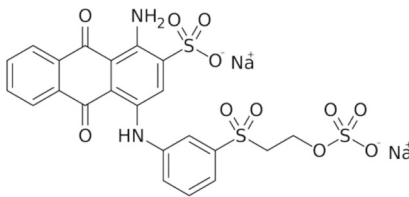
### Characterization methods

Fourier-transform infrared spectroscopy (FTIR) was used to identify the functional groups present on the surface of *Bifurcaria bifurcata* (Bif-Bcata) alga. The crushed Bif-Bcata was analyzed by a FT-IR 8400S spectroscope (Shimadzu). The spectrum was recorded between 4000 and 500 cm<sup>-1</sup> (4-cm<sup>-1</sup> resolution, 64 sweeps).

The morphology and elementary composition of Bif-Bcata were characterized using a Hitachi S3400N scanning electron microscope equipped with an X-ray energy spectrometer (EDS) dispersion with an acceleration beam of 15 kV.

The determination of pH zero-point charges (pH<sub>ZPC</sub>) was carried out by preparing several solutions (volume = 50 mL) of NaCl (0.01 M) in a closed Erlenmeyer flask and adjusting the pH of each solution to values between 2 and 10 by adding NaOH or HCl (1 M). The same amount of Bif-Bcata (mass = 50 mg) was added to each of the Erlenmeyer, which are then stirred at 25 °C for 24 h. Finally, the final pH of each Erlenmeyer flask is measured. The initial pH is represented as a function of the final pH, and the point of zero charges

**Table 1** The main characteristics of MB and RB19 dyes

	Methylene Blue	Reactive Blue 19
<b>Empirical formula</b>	C <sub>16</sub> H <sub>18</sub> ClN <sub>3</sub> S	C <sub>22</sub> H <sub>16</sub> N <sub>2</sub> Na <sub>2</sub> O <sub>11</sub> S <sub>3</sub>
<b>Molecular weight (g/mol)</b>	319.85	626.54
<b>λ<sub>max</sub> (nm)</b>	664	590
<b>Chemical structure</b>		
<b>CAS Number</b>	61-73-4	2580-78-1



**Fig. 1** The *Bifurcaria bifurcata* crude material

(120 min). For each dose, equilibrium concentration was measured and the uptake percentage and adsorption capacity were calculated.

### Effect of solution pH

Fifty milliliters of 10 mg/L MB or RB19 solution was shaken for 120 min at a temperature of 25 °C, with a constant amount of biosorbent (0.02 g for MB and 0.1 g for RB19) and at different pH values. The pH was adjusted either with the addition of diluted HCl or NaOH. For each pH value, equilibrium concentration was measured, and then the uptake percentage and adsorption capacity were calculated.

(pH<sub>zpc</sub>) is the point where the curve pH final versus initial pH crosses the line pH initial = pH final (Zbair et al. 2018b).

## Biosorption experiments

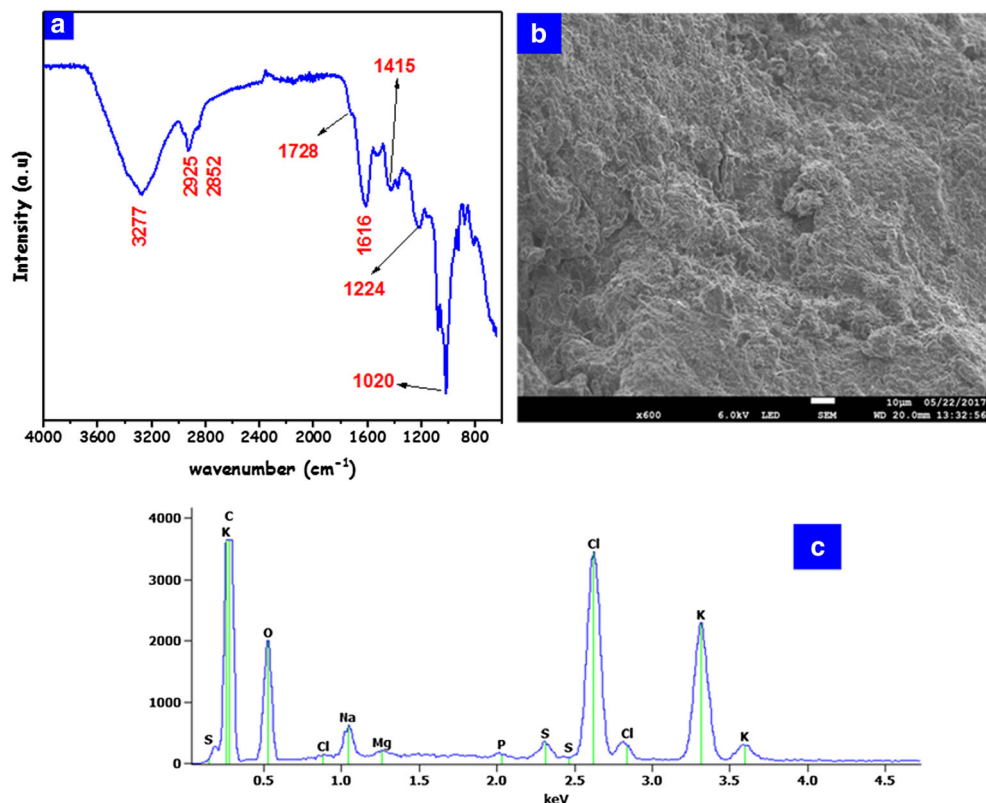
### Effect of biosorbent mass

Fifty milliliters of 10 mg/L MB or RB19 solution was added to variable biosorbent masses at a fixed pH = 5.6 (MB) and pH = 1 (RB19), temperature (25 °C), and shaking time

### Effect of contact time

A mass of Bif-Bcata (0.02 g for MB and 0.1 g for RB19) was added to 50 mL of aqueous MB or RB19 solution (10, 30, and 60 mg/L) and stirred at 200 rpm to study the effect of contact time (0 to 120 min). After predetermined time intervals, the mixture of Bif-Bcata and MB or RB19 was immediately separated and analyzed by a UV-Visible spectrophotometer to measure the absorbance and calculate the residual concentration in solution.

**Fig. 2** Characterization of Bif-Bcata: FTIR (a); SEM image (b); EDS (c) analysis



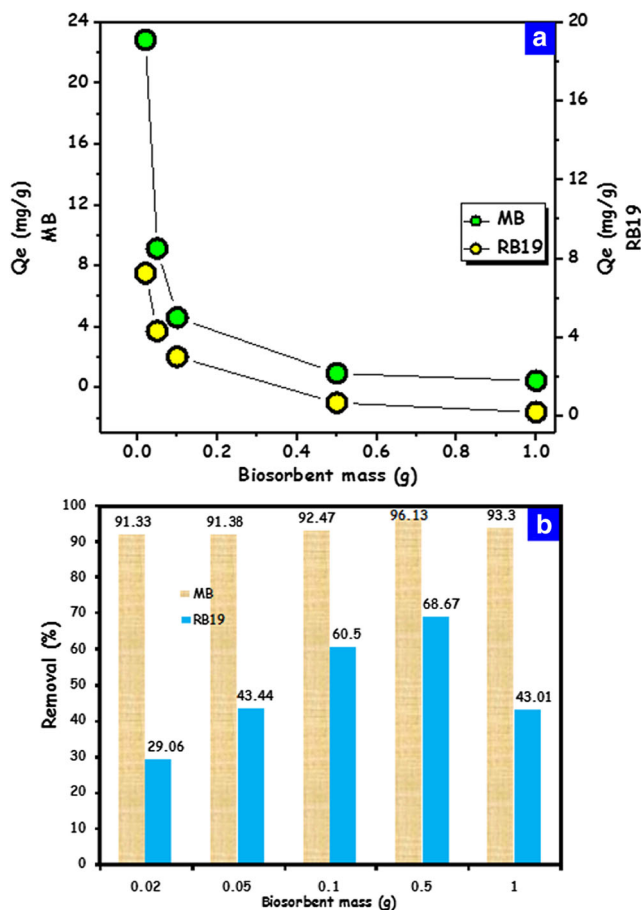


**Fig. 3** a Effect of biosorbent mass on the amount adsorbed of MB and RB19. b Effect of biosorbent mass on the removal efficiency of MB and RB19 ( $V = 50$  mL;  $C_0 = 10$  mg/L;  $t = 2$  h; pH = 5.6 (MB); pH = 1 (RB19);  $T = 25$  °C)

(RB19)). The mixture was shaken at a constant temperature for a fixed period of time. The solution was then filtered and the concentrations of MB or RB19 before and after adsorption were measured using a UV-Visible spectrophotometer. Based on the experimental results, many indicators were determined and two isotherm models (Langmuir and Freundlich) were studied using the obtained data.

The amount of MB and RB19 biosorbed at equilibrium expressed in terms of milligrams per gram and the removal efficiency is given in percentage were evaluated using the following equations (Al-Zboon et al. 2011):

$$Q_e = \frac{(C_0 - C_e)}{m} \times V$$

$$\%(\text{Removal}) = \frac{(C_0 - C_e)}{C_0} \times 100$$

where:

$Q_e$  the amount adsorbed in milligrams of adsorbate per gram of adsorbent

$C_0$  the initial concentration of MB or RB19 in milligrams per liter

$C_e$  the residual concentration of MB or RB19 in milligrams per liter

$m$  the adsorbent amount expressed in grams

$V$  the solution volume of MB or RB19 in liters

### Effect of the initial concentration

The effect of initial concentration on the adsorption of MB or RB19 by Bif-Bcata was investigated employing different concentrations of MB or RB19 ranging from 0 to 1000 mg/L at pH values 5.6 (MB) and 1 (RB19), and Bif-Bcata dosage of 0.02 g for MB and 0.1 g for RB19; the solution was then shaken for 120 min at a temperature of 25 °C. For each initial concentration, equilibrium concentration was measured, and then the uptake percentage and adsorption capacity were calculated.

### Adsorption isotherm

The study of MB or RB19 adsorption isotherms on the Bif-Bcata was carried out using batch equilibrium technique according to the following procedure: 50.0 mL of MB or RB19 solutions (10–1000 mg/L) was added to a fixed mass of Bif-Bcata of 0.02 g for MB and 0.1 g for RB19 at optimized pH (pH = 5.6 (MB) and pH = 1

## Results and discussion

### Characterization of Bif-Bcata

#### Fourier-transform infrared spectroscopy

The FTIR spectra of Bif-Bcata biosorbent (Fig. 2a) show several peaks which means that this biosorbent is rich in functional groups that can be an advantage in biosorption process. The broadband centered at 3277  $\text{cm}^{-1}$  indicates the presence of OH groups on Bif-Bcata surface. The two weak signals observed at 2925 and 2852  $\text{cm}^{-1}$  are associated with C–H groups. Furthermore, the peak noticed at around 1728 is recognized to C=O groups (Zbair et al. 2018e). Besides, the intense band at 1616  $\text{cm}^{-1}$  is related to asymmetric stretching of carboxylate O–C–O (Kloareg 1991). Also, the bands positioned at 1415, 1224, and 1020  $\text{cm}^{-1}$  might be assigned to

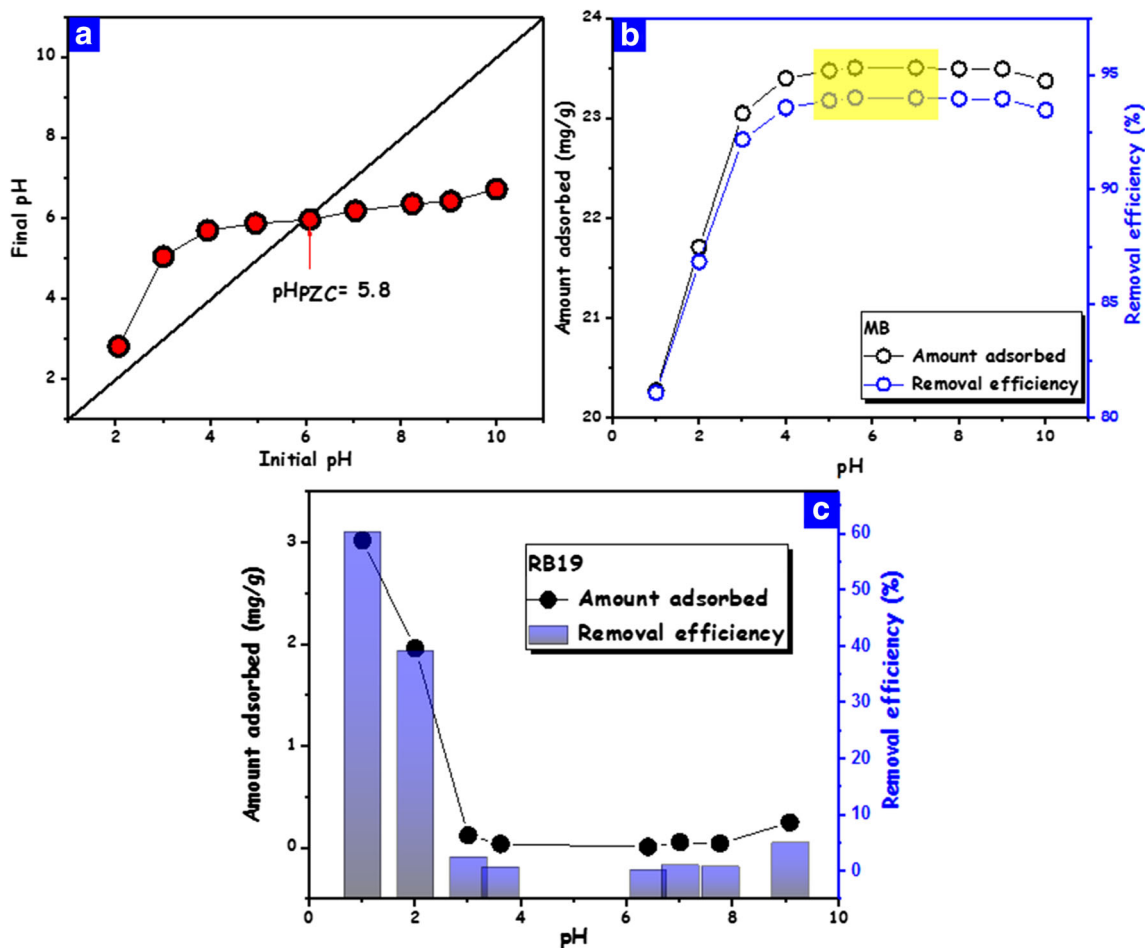


Fig. 4 a Determination of point zero charges (pHPZC). b Effect of pH on MB biosorption. c Effect of pH on RB19 biosorption

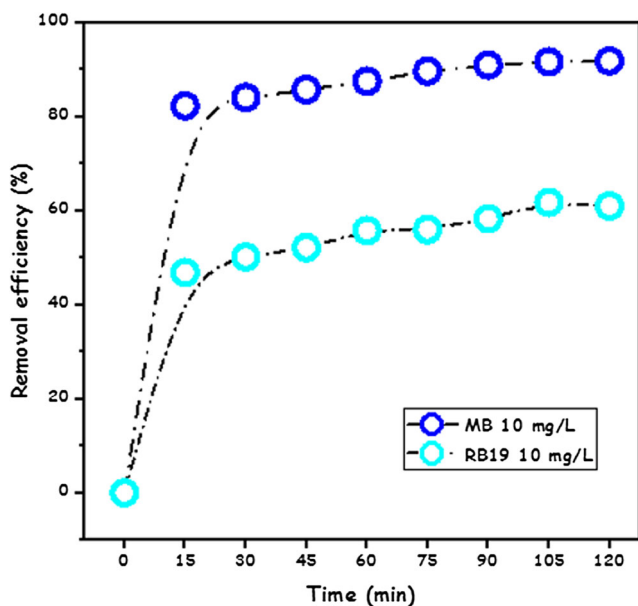


Fig. 5 Effect of contact time on the biosorption of MB and RB19 onto *Bifurcaria bifurcata* alga ( $V = 50$  mL;  $m$  (alga) = 20 mg (MB);  $m$  (alga) = 100 mg (RB19); pH = 5.6 (MB); pH = 1 (RB19);  $T = 25$  °C)

C–C–H and O–C–H deformation, C–O stretching, C–O and C–C stretching vibrations of pyranose rings, and sulfates groups (Kloareg 1991).

### Scanning electron microscopy

The morphological characteristic of *Bifurcaria bifurcata* (Bif-Bcata) alga was evaluated by a scanning electron microscope. The micrographs of Bif-Bcata and the EDS analysis are shown in Fig. 2b, c, respectively. Figure 2 b shows a rather irregular and nonporous material.

### EDS analysis

The EDS analysis presented in Fig. 2c shows the presence of C, O, Cl, K, Na, Mg, P, and S in Bif-Bcata alga. These elements are in different quantities. Indeed, the amount of C, O, Cl, and K is very high, whereas that of Na, Mg, P, and S is lower.

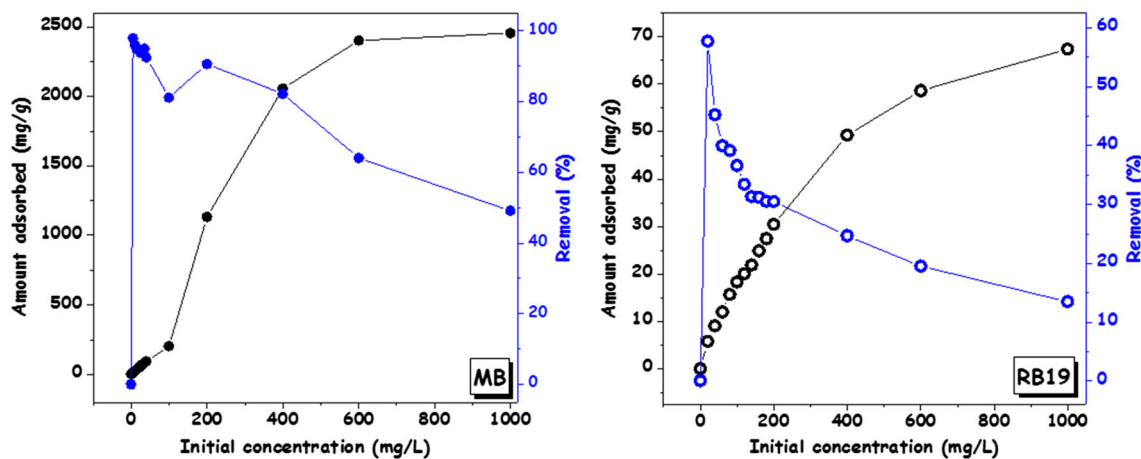


Fig. 6 Effect of MB and RB19 initial concentration on the biosorption capacity of *Bifurcaria bifurcata* alga ( $V = 50$  mL;  $m$  (alga) = 20 mg (MB) and 100 mg (RB 19); pH = 5.6 (MB), 1 (RB19);  $t = 2$  h;  $T = 25$  °C)

### MB and RB19 removal studies

#### Effect of biosorbent mass

Figure 3 a indicates that the Bif-Bcata dose has an effect on the amount of biosorbed dyes (MB or RB19). For MB, the amount biosorbed at equilibrium ( $Q_e$ ) decreases rapidly from 22.8 to 4.6 mg/g in the range from 0.02 to 0.1 g of Bif-Bcata mass and then continues to decrease slowly until it reaches 0.5 g where an equilibrium plateau begins to appear. Concerning RB19, we can observe a similar behavior, a rapid decrease in the amount biosorbed from 7.2 to 3 mg/g in an interval of Bif-Bcata mass ranging from 0.02 to 0.1 g. Then, it keeps decreasing slowly until 0.5 g where we start to see an equilibrium plateau.

Figure 3 b shows that the Bif-Bcata dose influences also the removal efficiency for both dyes. When the mass of Bif-Bcata was varied from 0.02 to 1 g, the removal efficiency of MB changes from 91.33 to 93.3% with a maximum of 96.13% removal corresponding to 0.5 g of Bif-Bcata, while the removal proficiency of RB19 changes from 29 to 43% with a maximum of 68.67% removal using the same amount of Bif-Bcata (0.5 g).

In fact, when we are working with a low Bif-Bcata masses (from 0.02 to 0.5 g), the removal efficiency increased by increasing the mass of Bif-Bcata; this can be explained by the availability of accessible sites in Bif-Bcata for MB or RB19. With increasing doses of Bif-Bcata ( $m > 0.5$  g), the number of adsorption sites can be increased, but MB and RB19 molecules have difficulties to approach these sites because of the congestion. The presence of the big amount of Bif-Bcata favors the agglomeration of particles, thus a diminution in the total surface area of Bif-Bcata and consequently a decrease in the adsorption capacity (Benzidia et al. 2015; Ouasfi et al. 2019a).

By analyzing the data of Fig. 3a, b, we notice the following conclusions:

- For MB biosorption, the high efficient removal obtained is 96% corresponding to 0.96 mg/g using 0.5 g of Bif-Bcata, while only 0.02 g of Bif-Bcata is sufficient to achieve an elimination percentage of 91% with an adsorption capacity of 22.8 mg/g (we loss 5% in adsorption efficiency, but 25 times more of Bif-Bcata mass was gained).
- For the biosorption of RB19 and following the same reason as before, we can notice that the optimal mass is 0.1 g corresponding to 60.5% of removal efficiency and 3 mg/g

Table 2 Non-linear equations of kinetic models

Kinetic model	Equation	Description	References
Pseudo-first-order	$Q_t = Q_{cal}(1 - \exp -K_1 t)$	$Q_t$ (mg/g): the amount adsorbed at time $t$ ; $Q_{cal}$ (mg/g): the amount adsorbed calculated at equilibrium; $K_1$ (1/min): the PFO rate constant; $t$ (min): the contact time	Lagergren (1898)
Pseudo-second-order	$Q_t = \frac{(K_2 Q_{cal}^2 t)}{(1 + K_2 Q_{cal} t)}$	$K_2$ (g/mg min): the PSO rate constant	Ho (2006)
Intraparticle diffusion	$Q_t = K_{ip} t^{1/2} + C$	$K_{ip}$ (mg/g min <sup>1/2</sup> ): rate coefficient; $C$ (mg/g): thickness of the boundary layer	Weber and Morris (1963)

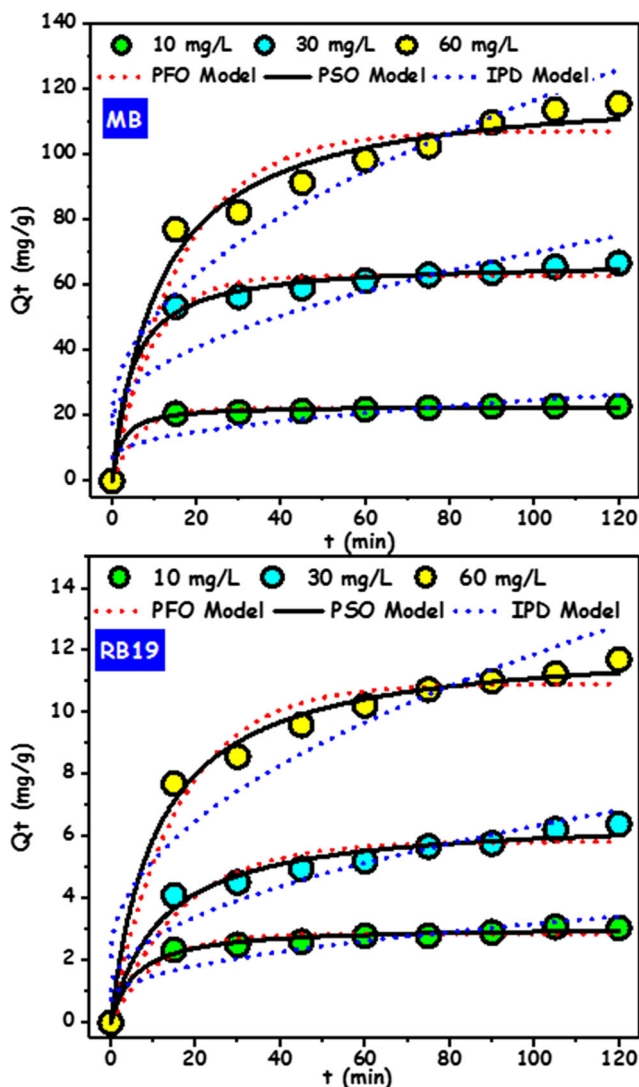


Fig. 7 Non-linear fit models (PFO, PSO, IPD) for MB and RB19 biosorption onto *Bifurcaria bifurcata* alga

of adsorption capacity (we lose about 8% of biosorption efficacy, but we gain 5 times more on biosorbent mass).

Finally, and in order to carry out the rest of our experiments, we have retained the following optimum masses of Bif-Bcata: 20 mg for MB and 100 mg for RB19.

### Effect of solution pH

In all biosorption studies, the pH remains an important factor, since it can influence both the structure of the biosorbent and the adsorbate but also the interaction mechanism (Tran et al. 2017c; Zbair et al. 2018c; Anfar et al. 2019). The surface charge of a given biosorbent will, therefore, depend on the pH and ionic strength of the solution which the material is contacted with (Tran et al. 2017a). This charge can be positive, negative, or null depending on the operating conditions (Zbair et al. 2018a). An important surface characteristic is point zero charges ( $pH_{PZC}$ ) that defines the pH for which the surface charge is null. The results obtained are summarized in Fig. 4.

At pH values lower than  $pH_{PZC}$  (zone before the intersection), we observe that the curve is above the straight line, which means that the Bif-Bcata surface charges are globally positive and at pH values higher than  $pH_{PZC}$  (zone just after the intersection), the curve is below the straight line; this indicates that the Bif-Bcata surface is negatively charged. The intersection of the curve with the straight line gives us the  $pH_{PZC}$  value which is equal to 5.8.

The effect of the solution pH on the biosorption efficiency of MB and RB19 dyes onto Bif-Bcata was studied by varying the pH between 1 and 10. The outcomes obtained are shown in Fig. 4b, c.

The analysis of the results in Fig. 4b indicates several different steps in the pH evolution. Indeed, it can be observed that at low pH values, the amount biosorbed of MB onto Bif-Bcata is relatively small. When the pH is between 1 and 4, the curve shows a rapid increase of  $Q_e$  until it reaches a value of 23.4 mg/g. Thereafter, the evolution was quasi constant between pH 5 and 6. Finally, a low decrease was observed between pH 6 and 10. The maximum biosorption is therefore situated at pH range between 5 and 6. Therefore, the optimal pH was 5.6 which corresponds to the best biosorption efficiency. Subsequently, we performed all next biosorption experiments of MB at this optimal pH value of 5.6.

At acidic pH, the biosorption of MB is low. The active sites on Bif-Bcata surface are poorly ionized and the concentration of  $[H_3O^+]$  is higher in solution favoring the protonation of these

Table 3 Kinetic model parameters (PFO, PSO, IPD) for MB adsorbed onto *Bifurcaria bifurcata* alga

$C_0$ (mg/L)	Pseudo-first-order				Pseudo-second-order			Intraparticle diffusion model		
	$Q_{e, \text{exp}}$ (mg/g)	$Q_{e, \text{cal}}$ (mg/g)	$K_1$ ( $\text{min}^{-1}$ )	$R^2$	$Q_{e, \text{cal}}$ (mg/g)	$K_2$ (g/mg min)	$R^2$	$K_{ip}$ (mg/g $\text{min}^{1/2}$ )	$C$ (mg $\text{g}^{-1}$ )	$R^2$
10	22.95	22.25	0.165	0.992	23.03	0.020	0.997	1.75	7.26	0.682
30	66.69	62.86	0.113	0.982	67.05	0.003	0.994	5.23	17.62	0.764
60	115.50	107.27	0.061	0.953	121.37	0.001	0.981	9.66	19.97	0.894

$C_0$  (mg/L): the initial concentration of MB or RB19;  $Q_{e, \text{exp}}$  (mg/g): the experimental amount adsorbed at equilibrium;  $Q_{e, \text{cal}}$  (mg/g): the amount adsorbed calculated at equilibrium

**Table 4** Kinetic model parameters (PFO, PSO, IPD) for RB19 adsorbed onto *Bifurcaria bifurcata* alga

$C_0$ (mg/L)	Pseudo-first-order				Pseudo-second-order			Intraparticle diffusion model		
	$Q_{e, \text{exp}}$ (mg/g)	$Q_{e, \text{cal}}$ (mg/g)	$K_1$ ( $\text{min}^{-1}$ )	$R^2$	$Q_{e, \text{cal}}$ (mg/g)	$K_2$ (g/mg min)	$R^2$	$K_{ip}$ (mg/g $\text{min}^{1/2}$ )	$C$ (mg $\text{g}^{-1}$ )	$R^2$
10	3.08	2.86	0.098	0.971	3.10	0.054	0.989	0.24	0.73	0.803
30	6.39	5.84	0.059	0.951	6.64	0.012	0.979	0.52	1.04	0.888
60	11.71	10.93	0.063	0.971	12.30	0.007	0.991	0.97	2.13	0.882

$C_0$  (mg/L): the initial concentration of MB or RB19;  $Q_{e, \text{exp}}$  (mg/g): the experimental amount adsorbed at equilibrium;  $Q_{e, \text{cal}}$  (mg/g): the amount adsorbed calculated at equilibrium

sites. Above  $\text{pH} = 2$ , the concentration of  $\text{H}^+$  decreases compared with that of cationic MB, resulting in an increase in the rate of biosorption. At a high pH greater than 5, the active sites are deprotonated allowing a high affinity for the cationic MB dye instead of  $\text{H}_3\text{O}^+$  ions (Anfar et al. 2017; Zbair et al. 2018d).

So at  $\text{pH} < \text{pH}_{\text{PZC}}$ , the MB molecule and the surface of Bif-Bcata are positively charged, which favors electrostatic repulsions and therefore, the adsorption efficiency is relatively low. For a pH between 5 and 6 ( $\text{pH}_{\text{PZC}} = 5.8$ ), the MB molecule and Bif-Bcata surface are not protonated, which favors electrostatic interactions, thus increasing the percentage of biosorption. At higher pH values ( $\text{pH} > \text{pH}_{\text{PZC}}$ ), the MB molecule is cationic whereas the Bif-Bcata surface is negative, which reinforces the biosorption either by electrostatic interaction or by dispersion and the biosorption rate remains almost constant. Above pH 9, MB is in a very basic medium, which explains the slight decrease in the adsorption rate (Hamdaoui and Chiha 2007).

Figure 4 c shows the pH effect on biosorption of RB19 onto Bif-Bcata. At  $\text{pH} = 1$ , the elimination efficiency is maximum and equal to 60.5%, which corresponds to 3 mg/g in biosorbed quantity. Then, at  $\text{pH} = 2$ , it decreases to 39.2%. Then, for pH values higher than 2, a dramatic decrease was observed and the removal efficiency is increased from 39.2 to about 1%. At basic pH, biosorption is not favorable. The maximum biosorption is observed at pH 1; therefore, the subsequence of our experimental work was performed at  $\text{pH} = 1$ .

At  $\text{pH} = 1$ , the biosorption of RB19 is maximum. The concentration of  $[\text{H}_3\text{O}^+]$  is high enough to allow the protonation of the RB19 sulfonate groups, which favors the interaction between the RB19 and the functional groups of the Bif-Bcata. Above  $\text{pH} = 2$ , the concentration of  $\text{H}^+$  is not sufficient to protonate RB19 anions, resulting in a rapid decrease in biosorption rate. At high pH, the active sites of the Bif-Bcata and the RB19 are strongly ionized so the biosorption is not favorable.

So for  $\text{pH} < \text{pH}_{\text{PZC}}$  ( $\text{pH} = 1$ ), the RB19 molecule that is normally anionic is found protonated in a strongly acidic medium and the surface of Bif-Bcata is positive. This situation favors non-electrostatic interactions between the RB19 functional groups and the surface of our adsorbent (Bif-Bcata) and consequently increases the efficiency of the biosorption. For a pH between 5 and 6 ( $\text{pH}_{\text{PZC}} = 5.8$ ), the RB19 molecule and the surface of Bif-Bcata are not protonated, which favors electrostatic repulsions, thus reducing the rate of biosorption. At higher pH values, the RB19 molecule is anionic while the surface of Bif-Bcata is negative, which further enhances electrostatic repulsions and maintains a very low biosorption rate.

**Effect of contact time**

The result shown in Fig. 5 illustrates the evolution of the biosorption efficiency of MB and RB19 by Bif-Bcata in the function of contact time. During the first 15 min, we observe that the biosorption efficiency increased rapidly to reach 82%

**Fig. 8** Non-linear isotherm models of MB and RB19 biosorbed onto *Bifurcaria bifurcata* alga ( $V = 50 \text{ mL}$ ;  $m$  (alga) = 20 mg (MB) and 100 mg (RB 19);  $\text{pH} = 5.6$  (MB), 1 (RB19);  $t = 2 \text{ h}$ ;  $T = 25 \text{ }^\circ\text{C}$ )

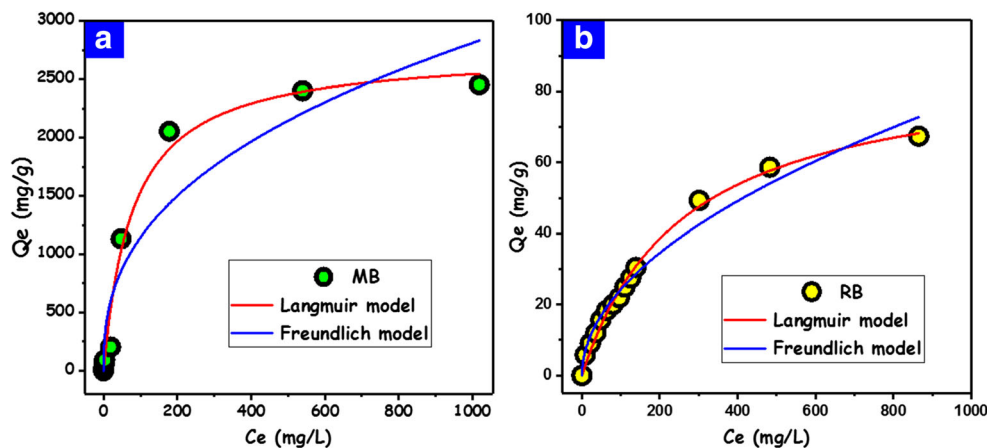




**Table 5** The non-linear equations of the Langmuir and Freundlich models

Models	Equation	Description	References
Langmuir	$Q_e = \frac{Q_{\max} K_L C_e}{1 + K_L C_e}$	$Q_e$ (mg/g): the amount adsorbed at equilibrium; $Q_{\max}$ (mg/g): the maximum adsorption capacity; $K_L$ (L/mg): the Langmuir constant; $C_e$ (mg/L): the concentration of adsorbate at equilibrium	Langmuir (1916)
	$R_L = \frac{1}{1 + K_L \times C_0}$	$K_L$ (L/mg) is the Langmuir constant and $C_0$ (mg/L) is the initial concentration. According to $R_L$ values, we can conclude that the adsorption is irreversible ( $R_L = 0$ ), favorable ( $0 < R_L < 1$ ), linear ( $R_L = 1$ ), or non-favorable ( $R_L > 1$ ).	Foo and Hameed (2010)
Freundlich	$Q_e = K_F C_e^{\frac{1}{n}}$	$K_F$ ((mg/g) (L/mg) <sup>1/n</sup> ): the Freundlich constant; $1/n$ : heterogeneity factor. According to the value of $1/n$ , the adsorption can be irreversible ( $1/n = 0$ ); non-favorable ( $1/n > 1$ ); favorable ( $0 < 1/n < 1$ )	Freundlich (1907)

and 47% for MB and RB19, respectively, then continues to increase moderately, before stabilizing and reaching equilibrium with a performance of 91.8% and 60.98% for MB and RB19, respectively.

Based on the results obtained in Fig. 5, it can be deduced that the biosorption kinetics of both dyes MB and RB19 is composed of two distinct steps. The first step is fast and indicates that the MB/RB19 adsorbs on easily accessible sites (external mass transfer), while the second step is slow and is characterized by a diffusion of MB/RB19 to less accessible sites (internal mass transfer) (Aarfane et al. 2014b; Ouasfi et al. 2019b).

### Effect of the initial concentration

The study of the effect of MB initial concentration on the adsorption capacity of Bif-Bcata was carried out by varying the MB concentration from 0 to 1000 mg/L. The results obtained are shown in Fig. 6. The curve indicates a rapid increase in biosorption capacity for concentrations ranging from 0 to 1000 mg/L. The retention capacity continues to improve with increasing initial concentration, indicating the existence of attraction forces between the Bif-Bcata surface and cationic MB. Then, an equilibrium plateau appears when the concentration reaches the value of 600 mg/L, which may reflect the saturation of the active sites involved in the biosorption process (Benzidia et al. 2015; Ouasfi et al. 2019a).

We have also studied the influence of the initial concentration of RB19 on the biosorption capacity of Bif-Bcata by operating this time with concentrations ranging from 0 to 1000 mg/L. The results obtained are illustrated in Fig. 6.

Figure 6 indicates that the biosorbed amount of RB19 increases rapidly from 20 to 400 mg/L. The biosorption capacity

continues to go up with the increase of the initial concentration without the appearance of the equilibrium plateau. This can be explained by the existence of a large number of active sites (Ahmad et al. 2015) on the Bif-Bcata surface that may be available to uptake RB19 at concentrations reaching 1000 mg/L or even higher. The same behavior was observed when using watermelon rinds (Ahmad et al. 2015) as adsorbent under experimental conditions pH = 2 and T = 30 °C.

### Kinetic study

It is very important to predict the rate at which the pollutant is removed (Tran et al. 2017b). Kinetic modeling of the biosorption process allows describing the possible biosorption mode, to quantify the amount biosorbed at equilibrium and also to evaluate the kinetics parameters (Foo and Hameed 2010).

Non-linear fitting of the pseudo-first-order (PFO), pseudo-second-order (PSO), and intraparticle diffusion (IPD) kinetic models was used to describe the biosorption kinetics of MB and RB19 on Bif-Bcata. The PFO, PSO, and IPD equations used in this study are presented in Table 2.

The initial concentrations of 10, 30, and 60 mg/L for MB and RB19 were chosen to study the biosorption kinetics (Fig. 7). According to the results obtained from the PFO and PSO kinetic models (Tables 3 and 4), it can be seen that for the biosorption kinetics of both dyes MB and RB19, the values of the regression coefficients  $R^2$  are closer to the unity in the case of PSO model. In addition, the amount biosorbed calculated theoretically ( $Q_e$ , cal) was found close to that found experimentally ( $Q_e$ , exp). Hence, the PSO model gives a better description of the biosorption kinetics of MB and RB19 onto Bif-Bcata.

**Table 6** Parameters of isotherms models of MB and RB19 biosorbed onto *Bifurcaria bifurcata* alga

	Langmuir model				Freundlich model		
	$Q_{\max}$ (mg/g)	$K_L$ (L/mg)	$R_L$	$R^2$	$K_F$ (mg/g) (L/mg) <sup>1/n</sup>	$n$	$R^2$
MB	2744.5	0.012	0.046	0.986	189.8	2.56	0.912
RB19	88.7	0.004	0.238	0.994	2.32	1.96	0.974

**Table 7** Comparison of the maximum adsorption capacities between the *Bifurcaria bifurcata* alga and other adsorbents cited in the literature for MB and RB19 dyes at  $T = 25\text{ }^{\circ}\text{C}$  using the Langmuir model

	Adsorbents utilized	$Q_{\max}$ (mg/g)	Solution pH	References
Methylene blue	<i>Bifurcaria bifurcata</i> seaweed	2744.5	pH = 5.6	This work
	Cotton industry waste	303	pH = 10	Tenev et al. (2019)
	H <sub>3</sub> PO <sub>4</sub> -treated eucalyptus leaves	194.347	pH = 8	Ghosh et al. (2019)
	Soybean hulls	169.90	pH = 7	Cusioli et al. (2019)
	<i>Wodyetia bifurcata</i> biochar	149.34	Not reported	dos Santos et al. (2019)
	Kaolinite clay	102.04	pH = 8	Anoop Krishnan et al. (2015)
	Palm leaflets	72.3	pH = 6	Zeghoud et al. (2019)
	Palm frond base	70.87	pH = 6	Zeghoud et al. (2019)
Reactive Blue 19	NiO nanoparticles	98.83	pH = 6.5	Monsef Khoshhesab and Ahmadi (2016)
	CCNTs	95.24	pH = 4	Hu et al. (2017)
	Z300 powder	89.3	pH = 4	Ada et al. (2009)
	<i>Bifurcaria bifurcata</i> seaweed	88.7	pH = 1	This work
	Bis aldehyde-functionalized silica gel	73.529	pH = 4	Banaei et al. (2017)
	Mg(OH) <sub>2</sub> -bentonite	66.9	pH = 2	Chinoune et al. (2016)
	Z075 powder	38.9	pH = 4	Ada et al. (2009)
	KSF-DP	30.76	Natural pH	Silva et al. (2012)

To study the transfer mechanism of dyes MB and RB19 on the surface of the alga Bif-Bcata, kinetic results were analyzed using the IPD model in its non-linear form. For both MB and RB19 dyes, the plot of the IPD model does not pass through the origin, which indicates the existence of some boundary layer effect (Al-Zboon et al. 2016). According to Fig. 7, at the beginning of the adsorption process, the rate is more important than the second step. The MB and RB19 dyes are firstly biosorbed on the external surface of Bif-Bcata. Subsequently, and after saturation of the external layer, the MB/RB19 could diffuse towards the internal active sites of Bif-Bcata but more slowly because of the increasing resistance to diffusion. These results led to conclude that the biosorption of MB and RB19 dyes onto Bif-Bcata took place in two stages: very fast chemical adsorption and slow intraparticle diffusion (Zbair et al. 2019b).

**Adsorption isotherms**

The biosorption isotherms studies of MB and RB19 were carried out to determine their modes of interaction with *Bifurcaria bifurcata* alga. The interpretation of the surface properties and biosorption capacities of the Bif-Bcata requires the modeling of equilibrium data by Langmuir and Freundlich models (Fig. 8). The Langmuir model assumes monolayer adsorption on a homogeneous surface composed of a limited number of identical sites. All sites are energetically equivalent and no interaction between the adsorbed molecules occurs (Langmuir 1916). On the other side, the Freundlich model supposes interactions between the adsorbed molecules, due

to multilayer adsorption on heterogeneous surfaces (Freundlich 1907). The non-linear equations of the Langmuir and Freundlich models are given in Table 5.

By comparing the correlation coefficients values ( $R^2$ ) (Tables 6), the  $R^2$  values indicate that the Langmuir model provides a better description of the experimental data. This means that the biosorption of MB and RB19 dyes onto Bif-Bcata occurs in monolayers on a homogeneous surface with the absence of any interaction between the adsorbed molecules (MB/RB19). Moreover, we also found an exceptional value of maximum biosorption capacity (2744.5 mg/g) of MB, while 88.7 mg/g in the case of RB19. In addition to that, the values of the parameter  $K_L$ , related to the affinity between MB/RB19 and Bif-Bcata, were equal to 0.012 L/mg and 0.004 L/mg for MB and RB19, respectively. This finding allows us to deduce that the active sites of Bif-Bcata have 3 times more affinity for the cationic dye MB than the anionic dye RB19. Another interesting parameter is also used to confirm the adsorption mode; it is  $R_L$  determined from the Langmuir model (please see Table 5).

From the results of Table 6, the  $R_L$  values were 0.046 and 0.238 for MB and RB19 adsorption, respectively. These two values, between 0 and 1, clearly prove that the biosorption of MB and RB19 onto Bif-Bcata is more favorable (Al-Harashsheh et al. 2015).

We have compared the biosorption capacity of our Bif-Bcata alga with other adsorbents already used and mentioned in the literature for the removal of the two dyes MB and RB19 (Table 7). It is obviously clear that with the exceptional value of  $Q_{\max} = 2744.5$  mg/g found for MB, our biosorbent is very effective and can be considered a material of choice for the

removal of cationic dyes. Furthermore, the adsorption capacity of 88.7 mg/g obtained for RB19 is compared with other adsorbents. Given these indications, the *Bifurcaria bifurcata* alga can be used efficiently to remove the impact of both cationic and anionic dyes from the environmental systems.

## Conclusion

During this work, we have studied the biosorption capability of two dyes MB and RB19, using a marine alga called *Bifurcaria bifurcata* (Bif-Bcata), which is widely available along the Moroccan Atlantic coastlines. The experimental results show that the biosorption process depends on the mass of Bif-Bcata, the initial dye concentration, and the pH of the solution. The optimal masses of Bif-Bcata were 20 mg and 100 mg for the biosorption of MB and RB19, respectively. The best adsorption efficiency was obtained at pH values 5.6 and 1 for MB and RB19, respectively. The kinetic study for biosorption of MB and RB19 follows the pseudo-second-order model. The modeling of biosorption isotherms revealed that the Langmuir model is more appropriate to describe the biosorption equilibrium, which means that the biosorption of MB and RB19 dyes onto Bif-Bcata occurs in monolayers on a homogeneous surface, with maximum biosorption capacities reaching 2744.5 mg/g and 88.7 mg/g for MB and RB19, respectively. Considering all these outcomes, we suggest that *Bifurcaria bifurcata* alga can be considered a promising biomaterial to be used as an effective adsorbent to remove pollution caused by cationic and anionic dyes often found in liquid effluents.

**Acknowledgments** The authors gratefully acknowledge the CUR CA2D and Littomer of Chouaib Doukkali University (El Jadida-Morocco) for their support. The authors would also like to thank Professors Charafeddine Jama (University of Lille) and Fouad Bentiss (Faculty of Sciences, UCD, El Jadida) for their valuable collaboration.

## Compliance with ethical standards

**Conflict of interest** The authors declare that they have no conflict of interest.

## References

- Aarfane A, Salhi A, El Krati M et al (2014a) Etude cinétique et thermodynamique de l'adsorption des colorants Red195 et Bleu de méthylène en milieu aqueux sur les cendres volantes et les mâchefers. *J Mater Environ Sci* 5:1927–1939
- Aarfane A, Salhi A, El Krati M et al (2014b) Kinetic and thermodynamic study of the adsorption of Red195 and methylene blue dyes on fly ash and bottom ash in aqueous medium. *J Mater Environ Sci* 5: 1927–1939
- Ada K, Ergene A, Tan S, Yalçın E (2009) Adsorption of Remazol Brilliant Blue R using ZnO fine powder: equilibrium, kinetic and

- thermodynamic modeling studies. *J Hazard Mater* 165:637–644. <https://doi.org/10.1016/j.jhazmat.2008.10.036>
- Ahmad MA, Ahmad N, Bello OS (2015) Removal of Remazol Brilliant Blue reactive dye from aqueous solutions using watermelon rinds as adsorbent. *J Dispers Sci Technol* 36:845–858. <https://doi.org/10.1080/01932691.2014.925400>
- Ait Ahsaine H, El Jaouhari A, Slassi A et al (2016) Electronic band structure and visible-light photocatalytic activity of Bi<sub>2</sub>WO<sub>6</sub>: elucidating the effect of lutetium doping. *RSC Adv* 6:101105–101114. <https://doi.org/10.1039/C6RA22669H>
- Ait Ahsaine H, Zbair M, Anfar Z et al (2018) Cationic dyes adsorption onto high surface area 'almond shell' activated carbon: kinetics, equilibrium isotherms and surface statistical modeling. *Mater Today Chem*. <https://doi.org/10.1016/j.mtchem.2018.03.004>
- Al-Harashsheh MS, Al Zboon K, Al-Makhadmeh L et al (2015) Fly ash based geopolymer for heavy metal removal: a case study on copper removal. *J Environ Chem Eng* 3:1669–1677. <https://doi.org/10.1016/j.jece.2015.06.005>
- Al-Zboon K, Al-Harashsheh MS, Hani FB (2011) Fly ash-based geopolymer for Pb removal from aqueous solution. *J Hazard Mater* 188:414–421. <https://doi.org/10.1016/j.jhazmat.2011.01.133>
- Al-Zboon KK, Al-smadi BM, Al-Khawaldh S (2016) Natural volcanic tuff-based geopolymer for Zn removal: adsorption isotherm, kinetic, and thermodynamic study. *Water Air Soil Pollut* 227:248–222. <https://doi.org/10.1007/s11270-016-2937-5>
- Anfar Z, El Haouti R, Lhanafi S et al (2017) Treated digested residue during anaerobic co-digestion of Agri-food organic waste: methylene blue adsorption, mechanism and CCD-RSM design. *J Environ Chem Eng* 5:5857–5867. <https://doi.org/10.1016/j.jece.2017.11.015>
- Anfar Z, Ait Ahsaine H, Zbair M, et al (2019) Recent trends on numerical investigations of response surface methodology for pollutants adsorption onto activated carbon materials: a review. *Crit Rev Environ Sci Technol* 1–42. doi: <https://doi.org/10.1080/10643389.2019.1642835>
- Anoop Krishnan K, Ajmal K, Faisal AK, Liji TM (2015) Kinetic and isotherm modeling of methylene blue adsorption onto kaolinite clay at the solid-liquid interface. *Sep Sci Technol* 50:1147–1157. <https://doi.org/10.1080/01496395.2014.965832>
- Badri N, Zbair M, Sahibed-Dine A et al (2018) Adsorption of cationic dyes by waste biomass treated by phosphoric acid. *J Mater Environ Sci* 9:1636–1644. <https://doi.org/10.26872/jmes.2018.9.6.182>
- Banaei A, Samadi S, Karimi S et al (2017) Synthesis of silica gel modified with 2,2'-(hexane-1,6-diylbis(oxy)) dibenzaldehyde as a new adsorbent for the removal of Reactive Yellow 84 and Reactive Blue 19 dyes from aqueous solutions: equilibrium and thermodynamic studies. *Powder Technol* 319:60–70. <https://doi.org/10.1016/j.powtec.2017.06.044>
- Ben Mansour H, Corroler D, Barillier D, Ghedira K, Chekir L, Mosrati R (2007) Evaluation of genotoxicity and pro-oxidant effect of the azo dyes: acids yellow 17, violet 7 and orange 52, and of their degradation products by *Pseudomonas putida* mt-2. *Food Chem Toxicol* 45: 1670–1677. <https://doi.org/10.1016/j.fct.2007.02.033>
- Ben Mansour H, Barillier D, Corroler D, Ghedira K, Chekir-Ghedira L, Mosrati R (2009) In vitro study of DNA damage induced by acid orange 52 and its biodegradation derivatives. *Environ Toxicol Chem* 28:489–495. <https://doi.org/10.1897/08-333.1>
- Benzidia N, Salhi A, Bakkas S, Khamliche L (2015) Biosorption of copper Cu (II) in aqueous solution by chemically modified crushed marine algae (*Bifurcaria bifurcata*): equilibrium and kinetic studies. *Mediterranean Journal of Chemistry* 4:85–92. <https://doi.org/10.13171/mjc.4.2.2015.08.04.11.19/khamliche>
- Benzidia N, Salhi A, Bentiss F et al (2017) Kinetics and equilibrium studies on biosorption of cadmium and lead ions from aqueous

- solutions by chemically modified algae *Bifurcaria bifurcata*. *J Mater Environ Sci* 8:4778–4784
- Chinoune K, Bentaleb K, Bouberka Z et al (2016) Adsorption of reactive dyes from aqueous solution by dirty bentonite. *Appl Clay Sci* 123: 64–75. <https://doi.org/10.1016/j.clay.2016.01.006>
- Cusioli LF, Quesada HB, Baptista ATA et al (2019) Soybean hulls as a low-cost biosorbent for removal of methylene blue contaminant. *Environ Prog Sustain Energy*. <https://doi.org/10.1002/ep.13328>
- DeVito SC (1993) Predicting azo dye toxicity. *Crit Rev Environ Sci Technol* 12:405–414. <https://doi.org/10.1080/10643389309388453>
- dos Santos KJL, dos Santos GE de Sá ÍMGLGL, et al (2019) *Wodyetia bifurcata* biochar for methylene blue removal from aqueous matrix. *Bioresour Technol* 293:122093. Doi: <https://doi.org/10.1016/j.biortech.2019.122093>
- El Atouani S, Belattmania Z, Reani A et al (2019) Brown seaweed *Sargassum muticum* as low-cost biosorbent of methylene blue. *Int J Environ Res* 13:131–142. <https://doi.org/10.1007/s41742-018-0161-4>
- Foo KY, Hameed BH (2010) Insights into the modeling of adsorption isotherm systems. *Chem Eng J* 156:2–10. <https://doi.org/10.1016/j.cej.2009.09.013>
- Freundlich H (1907) Über die adsorption in Lösungen. *Z Phys Chem* 57U. <https://doi.org/10.1515/zpch-1907-5723>
- Ganesh R, Boardman GD, Michelsen D (1994) Fate of azo dyes in sludges. *Water Res* 28:1367–1376. [https://doi.org/10.1016/0043-1354\(94\)90303-4](https://doi.org/10.1016/0043-1354(94)90303-4)
- Ghosh K, Bar N, Biswas AB, Das SK (2019) Removal of methylene blue (aq) using untreated and acid-treated eucalyptus leaves and GA-ANN modelling. *Can J Chem Eng* 97:2883–2898. <https://doi.org/10.1002/cjce.23503>
- Haffad H, Zbair M, Anfar Z et al (2019) Removal of reactive red-198 dye using chitosan as an adsorbent: optimization by central composite design coupled with response surface methodology. *Toxin rev* 1–13. doi: <https://doi.org/10.1080/15569543.2019.1584822>
- Hamdaoui O, Chihha M (2007) Removal of methylene blue from aqueous solutions by wheat bran. *Acta Chim Slov* 54:407–418
- Ho Y-S (2006) Review of second-order models for adsorption systems. *J Hazard Mater* 136:681–689. <https://doi.org/10.1016/j.jhazmat.2005.12.043>
- Hu C, Hu N, Li X et al (2017) Adsorption of remazol brilliant blue R by carboxylated multi-walled carbon nanotubes. *Desalin Water Treat* 62:282–289. <https://doi.org/10.5004/dwt.2017.20145>
- Kloareg PB (1991) Structure and propriétés d'échange des parois cellulaires des algues brunes. Implications écophysiologicals. *Bull la Soc Bot Fr Actual Bot* 138:305–318. <https://doi.org/10.1080/01811789.1991.10827076>
- Lakshmiopathy R, Sarada NC (2016) Methylene blue adsorption onto native watermelon rind: batch and fixed bed column studies. *Desalin Water Treat* 25:10632–10645. <https://doi.org/10.1080/19443994.2015.1040462>
- Langmuir I (1916) The constitution and fundamental properties of solids and liquids. Part I Solids *J Am Chem Soc* 38:2221–2295. <https://doi.org/10.1021/ja02268a002>
- Lazim ZM, Mazuin E, Hadibarata T, Yusop Z (2015) The removal of methylene blue and Remazol Brilliant Blue R Dyes by using orange peel and spent tea leaves. *J Teknol* 74:129–135. <https://doi.org/10.11113/jt.v74.4882>
- Mafra MR, Igarashi-Mafra L, Zuim DR et al (2013) Adsorption of remazol brilliant blue on an orange peel adsorbent. *Braz J Chem Eng* 30:657–665. <https://doi.org/10.1590/S0104-66322013000300022>
- Monsef Khoshhesab Z, Ahmadi M (2016) Removal of reactive blue 19 from aqueous solutions using NiO nanoparticles: equilibrium and kinetic studies. *Desalin Water Treat* 57:20037–20048. <https://doi.org/10.1080/19443994.2015.1101713>
- Ouasfi N, Bouzekri S, Zbair M et al (2019a) Carbonaceous material prepared by ultrasonic assisted pyrolysis from algae (*Bifurcaria bifurcata*): response surface modeling of aspirin removal. *Surfaces and Interfaces* 14:61–71. <https://doi.org/10.1016/j.surfin.2018.11.008>
- Ouasfi N, Zbair M, Bouzikri S et al (2019b) Selected pharmaceuticals removal using algae derived porous carbon: experimental modeling and DFT theoretical insights. *RSC Adv* 9:9792–9808. <https://doi.org/10.1039/C9RA01086F>
- Silva MMF, Oliveira MM, Avelino MC et al (2012) Adsorption of an industrial anionic dye by modified-KSF-montmorillonite: evaluation of the kinetic, thermodynamic and equilibrium data. *Chem Eng J* 203:259–268. <https://doi.org/10.1016/j.cej.2012.07.009>
- Tenev MD, Farias A, Torre C et al (2019) Cotton industry waste as adsorbent for methylene blue. *J Sustain Dev Energy, Water Environ Syst* 7:667–677. <https://doi.org/10.13044/j.sdewes.d7.0269>
- Tran HN, Chao HP (2018) Adsorption and desorption of potentially toxic metals on modified biosorbents through new green grafting process. *Environ Sci Pollut Res* 25:12808–12820. <https://doi.org/10.1007/s11356-018-1295-9>
- Tran HN, Chao H-P, You S-J (2017a) Activated carbons from golden shower upon different chemical activation methods: synthesis and characterizations. *Adsorpt Sci Technol* 36:95–113. <https://doi.org/10.1177/0263617416684837>
- Tran HN, You SJ, Hosseini-Bandegharai A, Chao HP (2017b) Mistakes and inconsistencies regarding adsorption of contaminants from aqueous solutions: a critical review. *Water Res* 120:88–116. <https://doi.org/10.1016/j.watres.2017.04.014>
- Tran HN, You SJ, Nguyen TV, Chao HP (2017c) Insight into the adsorption mechanism of cationic dye onto biosorbents derived from agricultural wastes. *Chem Eng Commun* 204:1020–1036. <https://doi.org/10.1080/00986445.2017.1336090>
- Weber WJ, Morris JC (1963) Kinetics of adsorption carbon from solutions. *J Sanit Engineering Div Proceedings Am Soc Civ Eng* 89:31–60
- Zbair M, Ainassaari K, Drif A, Ojala S, Bottlinger M, Pirlä M, Keiski RL, Bensitel M, Brahmı R (2018a) Toward new benchmark adsorbents: preparation and characterization of activated carbon from argan nut shell for bisphenol A removal. *Environ Sci Pollut Res* 25:1869–1882. <https://doi.org/10.1007/s11356-017-0634-6>
- Zbair M, Ainassaari K, El Assal Z et al (2018b) Steam activation of waste biomass: highly microporous carbon, optimization of bisphenol A, and diuron adsorption by response surface methodology. *Environ Sci Pollut Res* 25:35657–35671. <https://doi.org/10.1007/s11356-018-3455-3>
- Zbair M, Anfar Z, Ait Ahsaine H et al (2018c) Acridine orange adsorption by zinc oxide/almond shell activated carbon composite: operational factors, mechanism and performance optimization using central composite design and surface modeling. *J Environ Manag*. <https://doi.org/10.1016/j.jenvman.2017.10.058>
- Zbair M, Anfar Z, Khallok H et al (2018d) Adsorption kinetics and surface modeling of aqueous methylene blue onto activated carbonaceous wood sawdust. *Fullerenes Nanotub Carbon Nanostructures* 26:433–442. <https://doi.org/10.1080/1536383X.2018.1447564>
- Zbair M, Bottlinger M, Ainassaari K, Ojala S, Stein O, Keiski RL, Bensitel M, Brahmı R (2018e) Hydrothermal carbonization of argan nut shell: functional mesoporous carbon with excellent performance in the adsorption of bisphenol A and diuron. *Waste and Biomass Valorization*:1–20. <https://doi.org/10.1007/s12649-018-00554-0>
- Zbair M, Ahsaine HA, Anfar Z, Slassi A (2019a) Carbon microspheres derived from walnut shell: rapid and remarkable uptake of heavy metal ions, molecular computational study and surface modeling. *Chemosphere* 231:140–150. <https://doi.org/10.1016/j.chemosphere.2019.05.120>
- Zbair M, Anfar Z, Ait Ahsaine H, Khallok H (2019b) Kinetics, equilibrium, statistical surface modeling and cost analysis of paraquat

removal from aqueous solution using carbonated jujube seed. RSC Adv 9:1084–1094. <https://doi.org/10.1039/C8RA09337G>

Zeghoud L, Gouamid M, Ben Mya O, Rebiai A, Saidi M (2019) Adsorption of methylene blue dye from aqueous solutions using two different parts of palm tree: palm frond base and palm leaflets.

Water Air Soil Pollut 230:195–199. <https://doi.org/10.1007/s11270-019-4255-1>

**Publisher's note** Springer Nature remains neutral with regard to jurisdictional claims in published maps and institutional affiliations.